Investigation of Postflooding Conditions in Countercurrent Gas–Liquid Flow

S. Maharudrayya and S. Jayanti
Dept. of Chemical Engineering, Indian Institute of Technology, Madras, Chennai 600 036, India

Systematic experiments were conducted to study the postflooding situation in air–water countercurrent flow in a tube of 0.025 m internal diameter with smooth inlet and outlet conditions for the two phases. The downflow rate of water and the pressure gradient were measured over a range of flow rates for test-section lengths of 0.6, 1.2 and 2.0 m. Additional experiments were conducted with increasing and decreasing water flow rates at a constant air flow rate. The length of the test section or the way the flooding point was approached did not significantly affect the onset of flooding. The data show that, as the gas flow rate is increased, the pressure gradient can fall significantly in the postflooding situation due to depleting the downflow rate of liquid. Dimensionless correlations are proposed to calculate the downflow rate and the pressure gradient given for overall flow parameters.

Introduction

In gas–liquid countercurrent flow in tubes, flooding can be considered as the upper limit of stable countercurrent flow; any increase in gas velocity will lead to destabilization of the flow, resulting in high-pressure drop and a diminished downflow rate of liquid. Further increase in the gas velocity will eventually lead to the drying out of the tube below the liquid injection, as all the liquid will be taken up by the gas. This point is known as the *flow-reversal point*, as the liquid flow is completely reversed from downward flow to upward flow. If the gas flow rate is reduced from that corresponding to flow reversal, a well-defined critical flow, which is usually lower than the flooding gas velocity, exists at that part of the liquid feed that flows downwards. This point is known as the deflooding point, and it can be considered as the lower limit of stable cocurrent flow in a tube. Further decrease of gas flow rate will lead to increasing the amount of feed flowing downwards until full countercurrent flow is reestablished. While studies of the flooding limit have a wide range of application, investigation of the postflooding condition has direct relevance to analyzing the safety systems of nuclear reactor cooling systems. One of the critical parameters to be studied in this context is the top flooding of a hot rod or a rod-bundle fuel element in a potential loss-of-coolant accident (LOCA) scenario (Collier, 1982). Here, the hot tube is quenched by coolant entering from the top. Due to the high temperature of the rod, coolant vapor is produced, setting up a countercurrent flow situation. The rate of advance of the coolant film front is limited by flooding. Much of the liquid-film flow would be governed by the *post* flooding hydrodynamic interaction between the liquid film and its vapor. Knowledge of the increased pressure gradient following flooding may also be used as a diagnostic tool in process plants.

While there have been a number of studies of countercurrent flow and the onset of flooding, there have been few systematic studies of the postflooding situation. Studies by Clift et al. (1966) have shown that the downflow curve, which is a variation of the net liquid downflow rate under postflooding conditions with gas flow rate, coincides with the deflooding curve, while studies by Zabaras and Dukler (1988) found that the downflow curve coincides with the flooding curve. Govan et al. (1991) reported results that indicated that the downflow curve lay above the flooding curve at low liquid flow rates, although, at high liquid flow rates, it lay below the flooding curve. The data available to date under these conditions are scant, and no measurements of the pressure gradient have been reported except in conditions near the flooding point. The purpose of the present work is therefore to investigate systematically the postflooding situation in countercurrent flow. To this end, new data of flooding, pressure drop, and downflow curves over a range of flow rates have been ob-

Correspondence concerning this article should be addressed to S. Jayanti.

tained in test sections of different lengths. These data are reported in the next section.

Experimental Details

The experimental setup used in the present study is shown in Figure 1. It consists of a transparent acrylic column having an internal diameter of 0.025 m and a total length of 4 m. Air is fed to the test section from one of two compressors (with maximum capacity of 8 m^3, 20 m^3 at STP conditions) connected in series. Water enters and exits from the test section through a filter assembly to provide smooth inlet and outlet conditions. The filter assembly consists of three elements: a stainless steel mesh that provides a large resistance to flow; a perforated cylindrical plate that provides rigidity to the mesh; and an outer cylinder that houses the two and is connected to the pump through a valve. The stainless steel mesh also consists of three layers—an inner layer of 25-micron mesh sandwiched between two layers of 100-micron mesh size. This combination mesh is wrapped tightly and tack welded onto the inside of a cylindrical plate that had an inner diameter slightly greater than that of the test section such that the whole assembly had an inner diameter equal to that of the test section. The perforated cylinder is fixed inside an acrylic cylinder with three nozzles to which flexible hoses are connected to feed water into the test section. The inner and outer cylinders are fixed rigidly between two flanges, and the whole assembly is connected to the test section to serve as the inlet for the water. The length of the test section, that is, the height between the water inlet and the water outlet, was 2.0 m. There was thus about 1 m length of pipe below and above the test section, which serves to provide a smooth inlet and outlet condition for air flow as well.

The static pressure in the test section was measured using a pressure gauge located in the middle of the test section. The pressure gradient over the test section was measured by using a carbontetrachloride-filled U-tube manometer. The water flow rate into the test section was measured using two rotameters with working ranges of 0–250 and 0–1000 liters per hour (l/h). The "excess" water flow rate through the top outlet under flooding and postflooding conditions was measured by collecting the water into a container for a known period of time. The volume of the collected water was measured using a graduated flask. The water downflow rate was obtained by taking the difference between total water input flow rate and the water flow rate through the top outlet. The air flow rate was measured by using an orifice meter.

Experiments were conducted for three test-section lengths, namely, 0.6, 1.2, and 2.0 m. In the first two cases, the bottom water outlet assembly was moved up to reduce the test-section length from the original length of 2.0 m. Pressure-gradient and downflow rate data were collected in the three test sections for water flow rate in the range 0.0070 to 0.083 kg/s (corresponding to a liquid-only Reynolds number in the range of 350 to 4500), and for air flow rate in the range of 0 to 0.009 kg/s, the latter corresponding to an air-only Reynolds number of 23,000. All the measurements were carried out at near atmospheric pressure and the test section pressure was less than 0.1 bar (gauge) in all cases. The ambient temperature was around 28°C during the experiments. In each case, the water flow rate was set at a particular value and the air flow rate was increased in small increments from a very low value. Once steady conditions were established, pressure-gradient and downflow rate measurements were conducted. Additional experiments were conducted in which the air flow rate was kept constant while the water flow was increased in small increments. In these experiments, measurements were also conducted for the case in which the water flow rate was *decreased* in small increments from an initially high value.

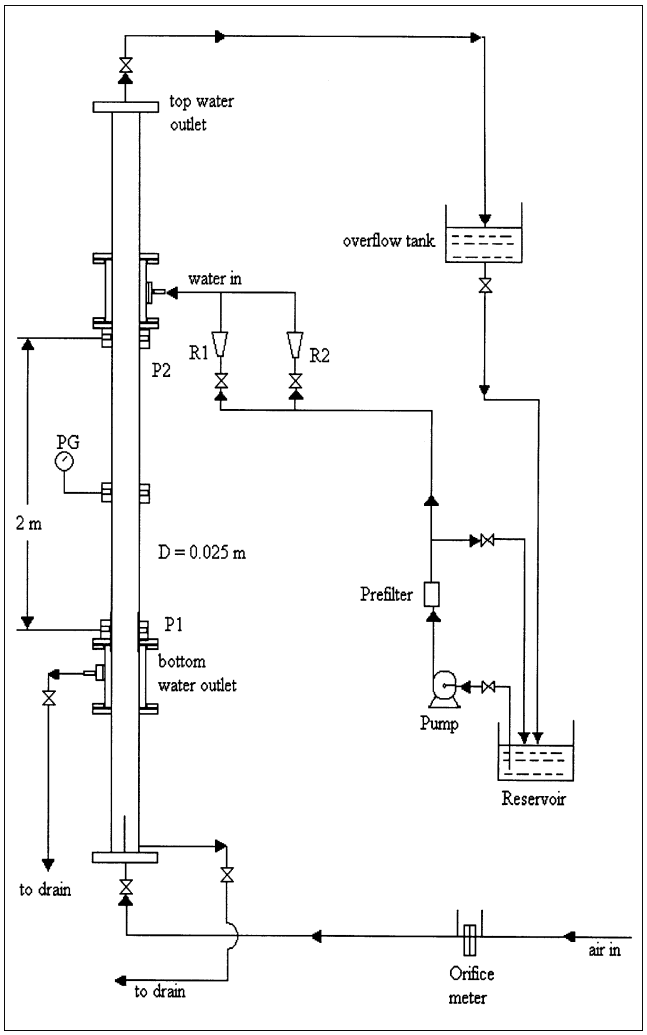

Figure 1. Experimental setup.

Results and Discussion

Typical results obtained from the experiments are shown in Figure 2, where the measured pressure drop (over a 1.2 m length of the test section) and the downflow rate are plotted against the air flow rate at a constant input water flow rate of 0.027 kg/s. The pressure drop increases rapidly at the flooding point and gradually decreases to a fraction of the value at flooding. The downflow rate curve shows a typically rapid decrease immediately after flooding followed by a gradual decrease further on.

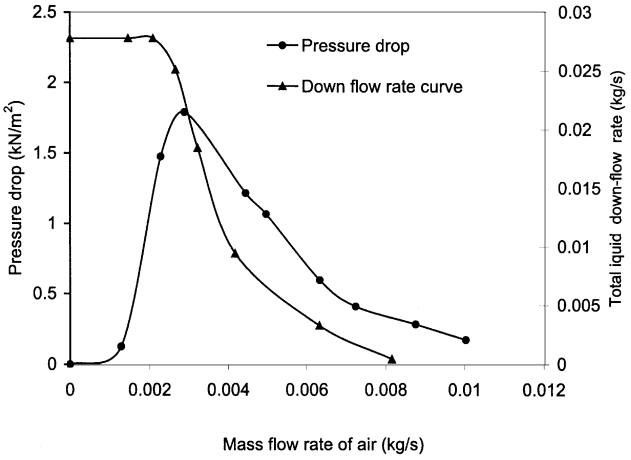

Figure 2. Pressure drop and the liquid downflow rate with air flow rate at a water flow rate of 0.027 kg/s in the 0.6-m-long test section.

Effect of test-section length on flooding

In the present study, experiments have been conducted in three different test-section lengths, such as 0.6 m, 1.2 m, and 2 m, in a tube with a 25-mm ID. There was no effect of the test section length on the mechanism of flooding. In all the cases, flooding occurred by the upward wave transport mechanism (Jayanti et al., 1996) with waves being carried upwards repeatedly from close to the bottom liquid outlet. There was very little entrainment of liquid in the form of droplets. As for the quantitative definition of the flooding gas velocity, this was taken as the gas velocity at which the pressure drop increased greatly and would correspond to point F in Figure 2. This was also the velocity at which the manometer showed large fluctuations. An average value was taken as the pressure gradient under these conditions. The data from the three test-section lengths are plotted in Figure 3 in terms of dimensionless flooding gas and liquid velocities, V_g^*, and V_l^*, respectively. These are given by

$$V_g^* = V_g\left(\frac{\rho_g}{Dg(\rho_l - \rho_g)}\right)^{0.5} \tag{1}$$

$$V_l^* = V_l\left(\frac{\rho_l}{Dg(\rho_l - \rho_g)}\right)^{0.5}. \tag{2}$$

There are a number of correlations in the literature to predict the onset of flooding, that is, to calculate the gas flow rate at which flooding would occur for a given liquid flow rate. Hewitt and Wallis (1963) correlated their data in terms of dimensionless liquid and gas superficial velocities

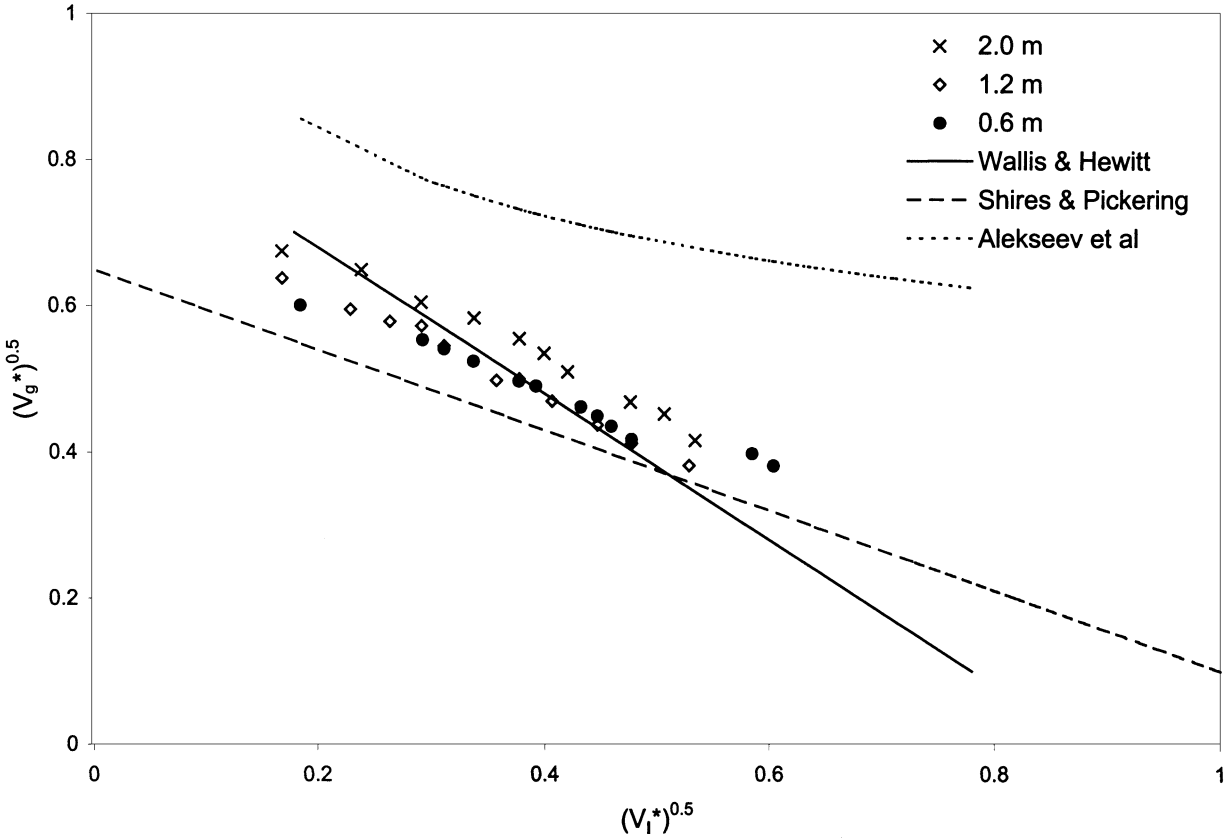

Figure 3. Experimental data of dimensionless gas velocity at flooding vs. prediction by correlations in test sections of lengths 0.6, 1.2 and 2.0 m.

$$\sqrt{(V_l^*)} + \sqrt{(V_g^*)} = C_1, \tag{3}$$

where the constant $C_1 = 0.88$ if $V_l^* < 0.3$, and is equal to 1.00 otherwise.

Shires and Pickering (1965) correlated their own data in a slightly modified form

$$\sqrt{(V_l^*)} + 0.55\sqrt{(V_g^*)} = 0.65. \tag{4}$$

Another type of empirical correlation was proposed by Alekseev et al. (1972) in terms of the Kutateladze number

$$K_g = 0.2576\, Fr^{-0.22}\, Bo^{0.26}, \tag{5}$$

where K_g, Fr, and Bo are the gas-phase Kutateladze number, Froude number, and Bond number, respectively, and are defined as

$$K_g = V_g\, \rho_g^{0.5} \left[g\sigma (\rho_l - \rho_g) \right]^{-0.25} \tag{6}$$

$$Fr = Q_l g^{0.25} (\rho_l - \rho_g)^{0.75} \sigma^{-0.75} \tag{7}$$

$$Bo = D^2 (\rho_l - \rho_g) g/\sigma. \tag{8}$$

The predictions of these correlations are also shown in Figure 3. It can be seen that the data from the different test-section lengths fall in a narrow band and are close to the Hewitt and Wallis predictions. Thus, the onset of flooding does not appear to be affected significantly by the change in the test-section length. While the data from the 0.6 m and 1.2 m test sections are nearly identical, the data from the 2.0-m-long test section are consistently, though only slightly, *higher* than those from these two. This behavior is rather unexpected in the light of the data of Hewitt et al. (1965), who show an opposite trend, namely, *decreasing* flooding gas velocity with increasing test section length. One possible reason for the discrepancy may lie in the way the state of flooding is achieved in the experiments. In the case of Hewitt and Wallis (1963), flooding is said to have been initiated by slight depressurization of the system. In the present experiments, no such depressurization was employed to initiate flooding. Rather, as the velocity approached the flooding limit, the countercurrent flow was found to become unstable near the liquid outlet, resulting in the formation of large waves that were periodically carried upwards. Prior to flooding, these large waves were not carried up all the way beyond the inlet; this occurred only with a further increase in the gas flow rate. Perhaps, sudden depressurization would have given these waves sufficient momentum to go beyond the liquid inlet. Since flooding required the appearance of liquid above the inlet, the depressurization technique would have detected flooding at a lower gas flow rate than the current method. Also, this discrepancy would be greater in a longer test section, which is consistent with the current results. In any case, the difference is small and is much less than the deviation in the predictions themselves. There have been other reports

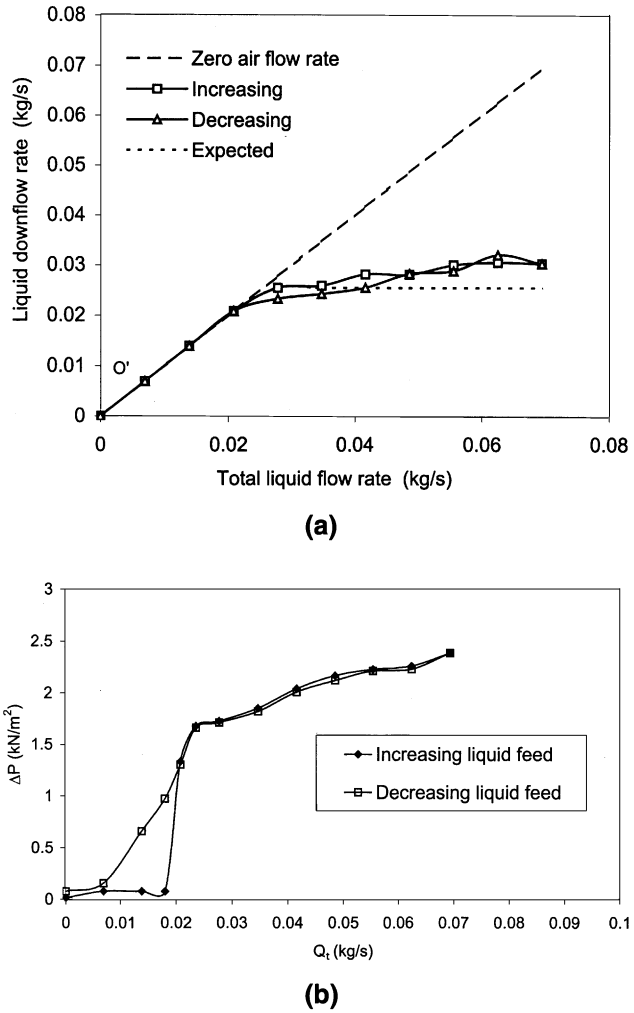

Figure 4. (a) Liquid downflow rate; (b) pressure drop with total 1 liquid flow rate at an air flow rate of 0.00209 kg/s for a test section length of 0.6 m.

where the effect of test-section length has been found to be negligible. Suzuki and Ueda (1977) found that the effect of test-section length was considerable in a 10 mm tube diameter, but much less so in an 18 mm tube diameter. Zabaras and Dukler (1988) could not detect any effect of length on flooding in their experiments in a tube diameter of 50.8 mm. Taking all these facts together, it can be concluded that the effect of the test-section length on the onset of flooding is small in the case of smooth entry conditions.

In order to verify the sensitivity of flooding to the way the flooding point is approached, additional experiments were conducted in the 0.6-m-long test section by keeping air flow rate constant ($m_g = 0.00209$ kg/s) and increasing the total (input) liquid flow rate, m_{lt}, from zero to a value considerably in excess of the flooding value. These increases were then followed by decreasing the input liquid flow rate to zero in small increments. The measured liquid downflow rate and the pressure gradient under these conditions are shown in Figures 4a and 4b, respectively. When the column was not flooded, the downflow was identical to the liquid input, so

that the condition in the column moved along the line $m_{ld} = m_{lt}$ (marked OA in Figure 4a). At the flooding point, the actual condition deviated from OA and tended toward the expected line of OA'. However, the measured liquid downflow rate exhibited a small increase with increasing liquid flow rate. The results from decreasing the water flow rate essentially followed the same curve, although the measured downflow rate tended to be slightly lower near the flooding transition. The pressure-drop variation between increasing and decreasing water flow rate showed a much more pronounced difference. As the water flow rate was increased, there was a small increase in pressure drop (see Figure 4b). The flooding point is characterized by the usual steep rise in the pressure drop, with a much more gradual increase and a further increase in the flow rate. The pressure-drop variation followed essentially the same curve when the water flow rate was decreased from the high value. However, at the flooding point, the pressure gradient did not show as sharp a fall as the rise shown while the flow rate increased. This can be attributed to the presence of churning motion (due to repeated carryover of large waves) being sustained in the test section under these conditions. The detection of the onset of flooding may be more difficult in this case, as the pressure gradient does not show as steep a change as in the case of increasing water flow rate.

From Figure 4, we find that the flooding water flow rate at a fixed air flow rate of 0.002 kg/s was about 0.025 kg/s. From Figure 2, we find that the flooding air flow rate at a fixed

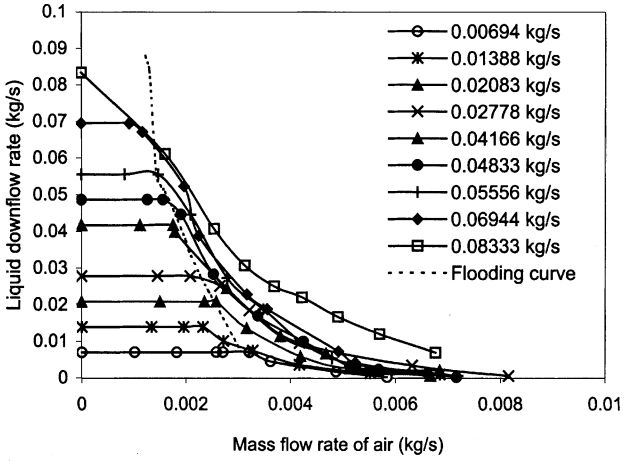

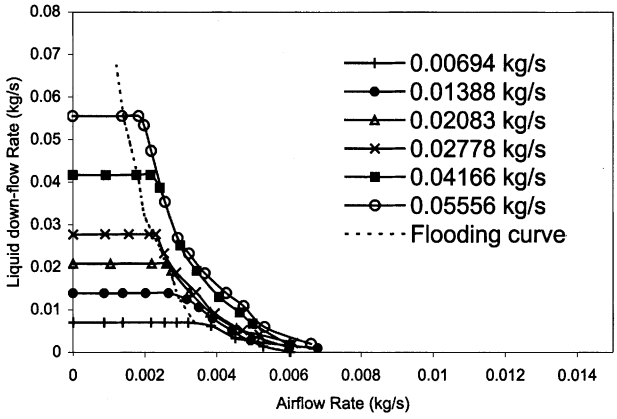

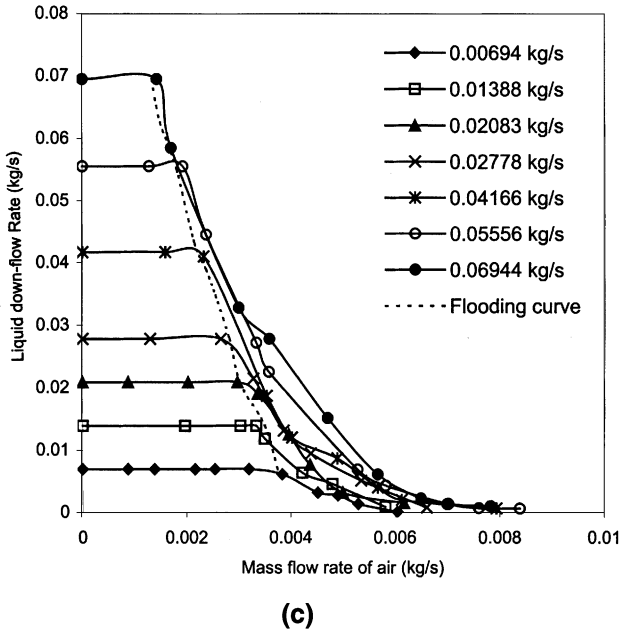

Figure 5. Liquid downflow rate with air flow rate for different total water input flow rates in a test section: (a) 0.6; (b) 1.2; and (c) 2.0 m length.

water flow rate of 0.027 kg/s was 0.02 kg/s. These results indicate that the flooding point remains nearly unchanged, that is, the flooding gas velocity is the same for a given liquid velocity. Thus, the initiation of flooding is largely insensitive to how the flooding point is approached. However, the postflooding situation appears to be different. Since maintaining a constant air flow rate over long periods is difficult, studies of the postflooding conditions were conducted by increasing the air flow rate while maintaining the water flow rate constant. The results from these experiments are discussed in the next section.

Downflow rate under postflooding conditions

In order to investigate the behavior of the column under flooded conditions, a number of runs were performed in test sections of different lengths, in which the liquid flow rate was kept constant while the air flow rate was increased in small increments. The measured downflow rate is plotted as a function of air flow in Figure 5 as the mass flow rate of the gas, m_g, was increased from zero to a value considerably in excess of the flooding value. It can be seen that, immediately after flooding, the downflow rate drops rapidly, followed by a more gradual decrease with a further increase in the air flow rate. Clift et al. (1966) reported a sudden drop in the downflow rate immediately after flooding, which was sometimes as much as 80% of the input liquid flow rate. Dukler et al. (1982) and Zabaras and Dukler (1988) obtained only a gradual decrease in the downflow rate when the air flow rate was increased, which is more consistent with the present data. Another interesting feature is that the flooding curve (which is obtained independently of these data but on the same rig) always lies below the downflow rate curve, the difference being more pronounced at high gas flow rates. This implies that the downflow rate in countercurrent flow at a given gas flow rate depends on whether or not flooding has occurred for that gas flow rate. Thus not all the excess input liquid, that is, the input liquid in excess of the flooding liquid flow rate at that gas flow rate, is carried away by the gas phase (a similar result is also seen in Figure 4a), and flooding therefore does not coincide with the point of maximum downflow rate of liquid at a given gas flow rate.

A number of such data were collected for a range of input water flow rates and are plotted in dimensionless form in Figure 6a in terms of dimensionless downflow rate, V_d', and dimensionless air flow rate, V_g', defined, respectively, as

$$V_d' = \frac{V_d}{V_l} \tag{9}$$

$$V_g' = \frac{V_g - V_{g,f}}{V_{g,do} - V_{g,f}}, \tag{10}$$

where V_d and V_l are the superficial downflow velocity and the superficial input flow velocity of liquid, respectively; $V_{g,f}$ is the gas velocity at the flooding point and $V_{g,do}$ is the gas velocity at complete dryout of the tube. However, $V_{g,do}$ has not been found in the present experiments, where conditions close to dryout conditions have been approached, but the dryout itself could not be achieved. Based on an extrapolation of the current data, the dryout condition is taken to be equal to $V_g^* = 1$, which is sometimes taken as the criterion for the onset of annular flow (Collier, 1981). It should be noted that under postflooding conditions, the dimensionless parameters, V_d' and V_g', vary between 0 and 1. The flooding point is represented by point (0,1) and the dryout point by the point (1,0) on the 2-D plot. The data were found to fall on a straight line if they were replotted in terms of $(V_d')^{0.6}$ and $(V_g')^{0.6}$, as shown in Figure 6b. This was correlated in the simple form

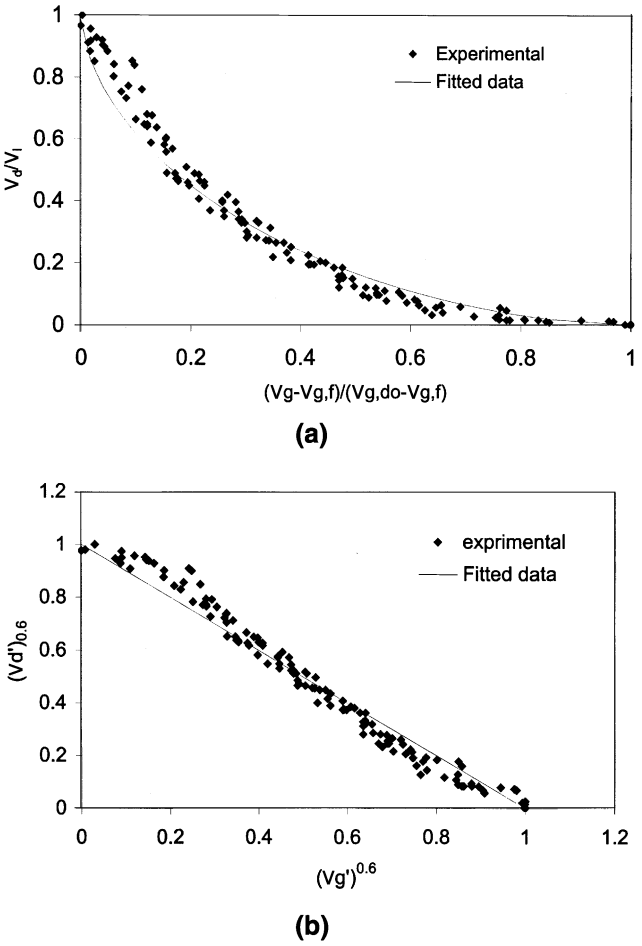

Figure 6. (a) Consolidated data of dimensionless liquid flow downflow rate with dimensionless air flow rate under postflooding conditions; (b) correlation of the postflooding downflow rate data.

$$(V_d')^{0.6} + (V_g')^{0.6} = 1.00. \tag{11}$$

The preceding correlation is drawn as a continuous line in Figure 6a and can be seen to give a good fit. Using this correlation, it is possible to determine the downflow rate for a given gas flow rate in postflooding conditions. The absolute error between the present data and with that of predicted values was found to be 27%.

As a validation of the preceding correlation, Eq. 11 was used to predict the downflow rate data of Zabaras and Duk-

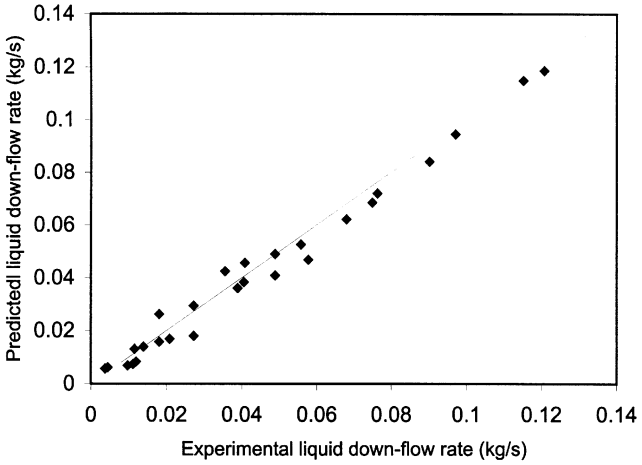

Figure 7. Experimental vs. predicted liquid downflow rates for the data by Zabaras and Dukler (1988) in a tube of 50.8 mm internal diameter.

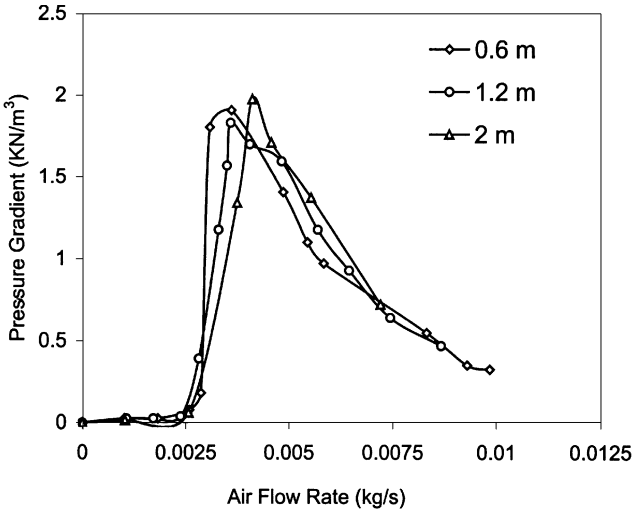

Figure 9. Variation of pressure gradient with air flow rate for different test section lengths at an input water flow rate of 0.00694 kg/s.

ler (1988) obtained in a 50.8-mm-dia. tube. These data were obtained at a fixed input liquid flow rate and a varying gas flow rate, as was done in the present study. The comparison between the predicted and the measured liquid downflow rate in the postflooding regime is shown in Figure 7. It can be seen that the agreement is quite good, with the average absolute error being 15%.

Pressure gradient under postflooding conditions

Typical variation in pressure drop with air flow rate at constant liquid flow rate under postflooding conditions is shown in Figure 8. The pressure drop typically exhibits a sudden and large increase, by an order of magnitude, following flooding for all liquid flow rates. Such large increases have also been reported by Hewitt et al. (1965) and Dukler et al. (1982), among others. The increased pressure drop in the test section is sustained with a further increase in the air flow rate, but it eventually decreases to a very low value as the liquid downflow rate becomes less.

The results obtained from test sections of different lengths show that the pressure drop is a strong function of the length of the test section. However, the pressure gradient itself does not vary significantly with the length. This is brought out clearly in Figure 9, where the pressure gradient obtained for different lengths is shown for a fixed water flow rate of 0.00694 kg/s. Thus, the pressure drop scales roughly with length. This is consistent with visual observations, which show that waves are repeatedly taken upwards from close to the liquid outlet onwards. Thus, whatever the test section length is, the liquid film structure is likely to be nearly the same. The interfacial friction, which is the dominant term in the pressure gradient under these conditions, is also therefore likely to be the same throughout the test section. If flooding is affected by length, which happens close to the liquid inlet, then one cannot expect the test section to have uniform structure along the length and the pressure gradient may show significant variation with length.

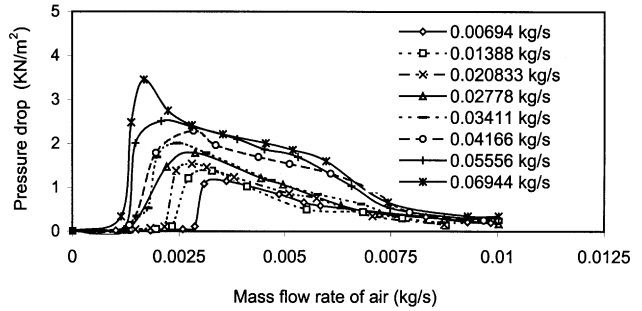

Figure 8. Pressure drop across the test section with air flow rate for different input water flow rates in a test section length of 0.6 m.

The insensitivity of the pressure gradient to the test section length allows the friction factor to be correlated in terms of the local flow variables, such as the phasic Reynolds numbers. There have been some previous attempts to determine the pressure gradient immediately after flooding (though systematic measurements such as above the pressure gradient under postflooding conditions have not been reported). Principal among these studies are those of Bharathan et al. (1979), Richter (1981), and Vijayan et al. (2001). Bharathan et al. evaluated the pressure gradient in terms of the interfacial friction factor, defined as

$$f_i = \frac{2\tau_i \alpha^2}{\rho_g V_g^2} = \frac{\left|\frac{-dp}{dz}\right| D\alpha^{2.5}}{2\rho_g V_g^2}, \qquad (12)$$

where τ_i is the interfacial shear stress and α is void fraction, which is related to film thickness by the relation

$$\alpha = \left(1 - \frac{2\delta}{D}\right)^2. \qquad (13)$$

To evaluate film thickness, Nusselt (1916) and Feind (1960) equations are used for laminar and turbulent flows, respectively

$$\delta^* = 1.442\ Re_f^{0.33} \quad \text{if} \quad Re_f < 400 \tag{14a}$$

$$\delta^* = 0.532\ Re_f^{0.5} \quad \text{if} \quad Re_f > 400, \tag{14b}$$

where Re_f is the liquid-film Reynolds number defined as the liquid mass flow rate per unit wetted perimeter divided by the dynamic viscosity, and δ^* is the dimensionless film thickness given by

$$\delta^* = \delta\left(\frac{\rho_l(\rho_l - \rho_g)g}{\mu_l^2}\right)^{1/3}. \tag{15}$$

Bharathan et al. (1979) proposed the following empirical correlation for f_i

$$f_i = 0.005 + 406\left(\frac{\delta}{D}\right)^{2.04}. \tag{16}$$

Application of this correlation to the present data shows significant scatter and a consistent underprediction by about 55% of the friction factor. Underprediction by nearly 90% has been observed for the correlation of Richter (1981).

Recently, Vijayan (2000) proposed a correlation for the pressure gradient immediately after flooding, based on a data bank consisting of his measurements in tubes of different diameters and data gathered from the literature. Vijayan expressed the interfacial friction in terms of the gas Reynolds number, the input liquid Reynolds number, diameter of the column, and the film thickness as

$$f_i = \frac{400\sqrt{Re_l}D^+\delta^+}{Re_g^{1.2}}, \tag{17}$$

where f_i, D^+, and δ^+ are given by

$$f_i = \frac{2\tau_i}{\rho_g V_g^2} = \frac{\left|\frac{-dp}{dz}\right|D}{2\rho_g V_g^2} \tag{18}$$

$$D^+ = \frac{D}{\sqrt{\left(\frac{\sigma}{(\rho_l - \rho_g)g}\right)}} \tag{19}$$

$$\delta^+ = \frac{\delta}{\sqrt{\left(\frac{\sigma}{(\rho_l - \rho_g)g}\right)}}. \tag{20}$$

The film thickness in Eq. 17 is obtained from a further correlation proposed by Vijayan

$$\delta_{pf} = 2.5\left[\frac{\delta^* Re_g^{0.1}}{Re_l^{0.15}D^{+0.31}}\right], \tag{21}$$

where δ^* is dimensionless film thickness and is calculated from Nusselt theory or from the correlation of Feind (1960), depending on the film Reynolds number (see Eqs. 14a and 14b).

Application of the Vijayan correlation to the present data shows an overprediction of about 60%. Thus, it appears that the correlations available for predicting the interfacial friction factor are unsuitable for postflooding conditions. Hence, a new correlation has been developed using the present data of 50 points obtained in postflooding conditions in a tube of 25 mm ID and for test-section lengths of 0.6, 1.2, and 2.0 m. Since the liquid downflow rate under postflooding conditions can be significantly different from the input liquid flow rate, the liquid Reynolds number based on the actual downflow rate (Re_d) was used as a parameter. Since the gas flow rate would have an effect on the friction factor, the gas Reynolds number, based on gas-only flow through the pipe, was taken as the third parameter. The correlation developed was of the following form

$$f_i = 15.7(Re_d)^{0.85}(Re_g)^{-0.4}(D^+)^{-1.7}, \tag{22}$$

where f_i is evaluated using Eq. 17 and D^+ is evaluated using Eq. 19. The exponent for the parameter D^+ was fixed based on comparison with the data obtained by Zabaras and Dukler (1988), in a tube diameter of 50.8 mm. A comparison of the predicted and the measured interfacial friction factor for the present data is shown in Figure 10a. Good agreement is obtained with an average absolute error of 28%. The correlation has also been used to predict the postflooding pressure gradient data given in Zabaras and Dukler (1988), and a comparison of the predicted and the experimental values for this case is shown in Figure 10b. The liquid downflow rate required in the correlation is obtained through the correlation developed earlier (see the section on downflow rate under postflooding conditions). It can be seen that excellent agreement is obtained with these data, too. While this does not serve as an entirely independent verification of the correlation (since the data were used in a limited way to fix the exponent for the D^+ parameter in Eq. 22), Figure 10 shows that data of the pressure gradient in tubes of different diameters can also be satisfactorily predicted.

Conclusions

Systematic experiments have been conducted to study the postflooding situation in gas–liquid countercurrent flow in a tube of 25-mm ID, with smooth inlet and outlet conditions

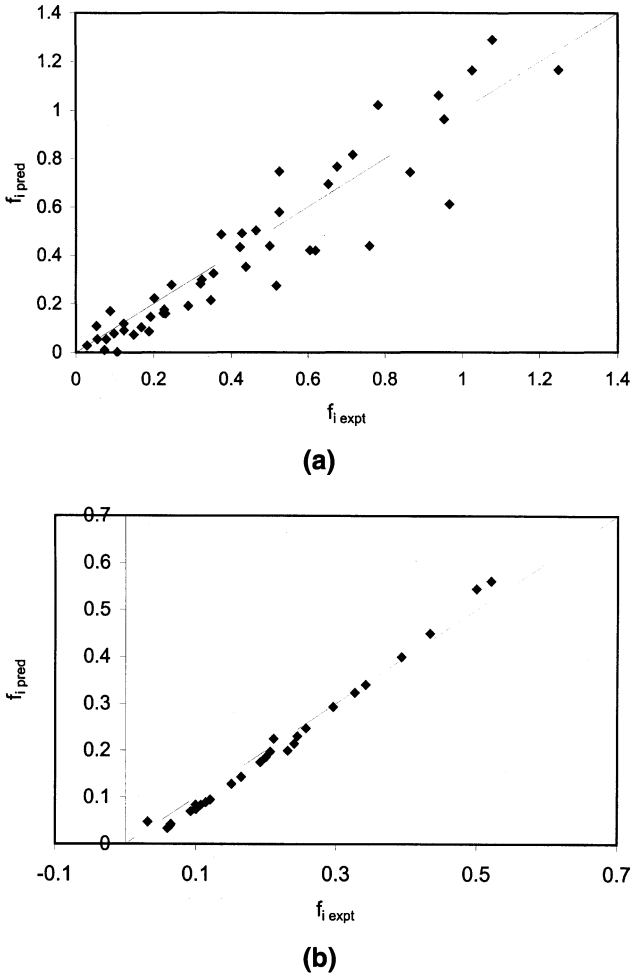

Figure 10. (a) Present data of interfacial friction factor vs. predictions of Eq. 22; (b) interfacial friction factor data of Zabaras and Dukler (1988) in a 50.8-mm-dia. tube with predictions of Eq. 22.

for the two phases. It is shown that the length of the test section, when varied between 0.6 and 2.0 m, did not have a significant effect on the onset of flooding. Data have been obtained for the downflow rate and the pressure gradient. These data show that, as the gas flow rate is increased, the pressure gradient can fall significantly in the postflooding situation due to a decrease in the downflow rate of the liquid. Dimensionless correlations have been proposed to calculate the downflow rate and the pressure gradient for the given overall flow parameters.

Literature Cited

Alekseev, V. P., A. E. Poberezkin, and P. V. Gerasimov, "Determination of Flooding Rates in Regular Packing," *Heat Transfer-Sov. Res.*, **4**, 159 (1972).

Bharathan, D., G. B. Wallis, and H. J. Richter, "Air-Water Countercurrent Annular Flow," Electric Power Research Institute Rep. EPRI-NP-1165, Palo Alto, CA (1979).

Clift, R. C., C. L. Pritchard, and R. M. Nedderman, "The Effect of Viscosity on Flooding Conditions in Wetted Wall Columns," *Chem. Eng. Sci.*, **21**, 87 (1966).

Collier, J. G., *Convective Boiling and Condensation*, 2nd ed., McGraw-Hill, New York (1981).

Collier, J. G., "Heat Transfer in the Postburnout Region and During Quenching and Reflooding," *Handbook of Multiphase Systems*, Chap. 6.5, G. Hetsroni, ed., Hemisphere, NY (1982).

Dukler, A. E., L. Smith, and A. Chopra, "Flooding and Upwards Film Flow in Tubes. I. Experimental Studies," *Int. J. Multiphase Flow*, **10**, 585 (1982).

Feind, F., "Falling Liquid Films with Countercurrent Air Flow in Vertical Tubes," *Ver. Deut. Ing.-Forschungsh.*, **481**, 26 (1960).

Govan, A. H., G. F. Hewitt, H. J. Richter, and A. Scott, "Flooding and Churn Flow in Vertical Pipes," *Int. J. Multiphase Flow*, **17**, 27 (1991).

Hewitt, G. F., and G. B. Wallis, "Flooding and Associated Phenomena in Falling Flow in a Vertical Tube," UKAEA, Harwell, Oxon, U.K., Rep. No. AERE R-4022 (1963).

Hewitt, G. F., P. M. C. Lacey, and B. Nicholls, "Transitions in Film Flow in a Vertical Tube," *Proc. Symp. Two-Phase Flow*, Exeter, UK (1965).

Jayanti, S., A. Tokarz, and G. F. Hewitt, "Theoretical Investigation of the Diameter Effect on Flooding in Countercurrent Flow," *Int. J. Multiphase Flow*, **22**, 307 (1996).

Nusselt, W., "Surface Condensation of Water Vapor," *Z. Ver. Deut. Ing.*, **60**(27), 541; also **60**(26), 569 (1916).

Richter, H. J., "Flooding in Tubes and Annuli," *Int. J. Multiphase Flow*, **7**, 647 (1981).

Shires, G. L., and A. R. Pickering, "The Flooding Phenomenon in Countercurrent Two-Phase Flow," *Proc. Symp. Two-Phase Flow*, Exeter, UK (1965).

Suzuki, K. H., and T. Ueda, "Behaviour of Liquid Films and Flooding in Countercurrent Two-Phase Flows: I: Flow in Circular Tubes," *Int. J. Multiphase Flow*, **3**, 517 (1977).

Vijayan, M., "Studies on the Hydrodynamics of Gas–Liquid Countercurrent Annular Flow," PhD Thesis, Indian Institute of Technology, Madras, India (2000).

Vijayan, M., S. Jayanti, and A. R. Balakrishnan, "Effect of Tube Diameter on Flooding," *Int. J. Multiphase Flow*, **27**, 797 (2001).

Zabaras, G. J., and A. E. Dukler, "Countercurrent Gas-Liquid Annular Flow Including the Flooding State," *AIChE J.*, **34**, 389 (1988).

Manuscript received Feb. 5, 2001, and revision received June 21, 2001.